

CHAPTER 9. Quench Protection

1. Introduction

The four CERN LHC interaction regions will consist of high gradient quadrupoles from KEK and the US-LHC accelerator project. The US magnets will be combined into a cryogenic element consisting of two 5.5 m quadrupoles connected in series by a superconducting bus bar. Superconducting busbar will also be used to connect this magnet element to the KEK magnets. The US magnets will operate at a peak field gradient of 215 T/m and corresponding excitation current of approximately 12 kA. Magnets will be equipped with strip heaters energized by external heater power. Upon the detection of a quench either from the magnet or the busbar, the leads of the magnet elements will be effectively shorted together and the heaters will be energized so that the stored energy will be dissipated within the magnet.

Adequate magnet protection means minimizing the peak coil temperature and minimizing the resistive-inductive voltage imbalances, which can generate large voltages to ground. As will be shown the protection of the magnet depends largely on the prompt and symmetric onset of resistive voltage due to the heaters after the quench is detected. The protection of the bus is dominated by the temperature growth prior to quench detection.

This chapter is thus divided into two parts. The first part deals with the quench protection of the magnet itself, driven by the optimization of the heater design within the framework of the LHC quench protection system. The second part deals with the design of the superconducting bus bar.

2. Parameters for Quench Protection System

Heater and bus bar designs are optimized within the constraints of the LHC quench protection. The design of the system has not been finalized. However, the following guide lines have been used.

- 1) Inner triplet magnets including the Fermilab built Q2, will utilize the CERN quench protection. System consists of quench detection circuitry and capacitance-based heater power supplies.

- 2) Detection of quench will be based on inferred resistive voltage growth. Voltage growth is measured from the subtraction of system inductive voltage. It is hoped that both the busbar and the magnet will be covered by the same quench detection electronics. The level of detection will be on the order of 300-500 mV.

3) In order to minimize spurious triggering, there will be approximately 10 ms of integration time for the inductance-subtracted voltage signals.

4) Magnet protection must contain redundancy. There will be two independent circuits/magnet element, each circuit capable of protecting the magnet circuit. If more than one heater/circuit, heaters should be powered in series.

5) Heater power supplies will consist of 7 mF capacitance and 900 V voltage. This will be accomplished by two banks of 14 mF capacitors charged to +/- 450 volts.

6) Within the constraints listed in "5)", the RC time constant of the heater circuit is dictated by the resistance of the heater and system resistance, and the heater energy density and heater peak power density is dictated by the resistance distribution in the heaters. Goals for the system are to have RC time constants comparable to the heater response time (typically less than 100 mS) and peak power densities of 20 W/cm² or greater [reference to ASC 96 paper on Quench Protection of IR Quads]

3. Magnet Protection/Heater Studies

As previously shown the superconducting quadrupoles consist of eight coils positioned in a two-layer $\cos(2\theta)$ coil geometry. The coils are electrically connected in series through inner coil pole turn to outer coil pole turn splices in each quadrant and through midplane turn quadrant to quadrant splices.

Heaters were placed in a magnet in groups of four, whose azimuthal positions on the outer layer are shown in Figure 1. The geometry of the heater is that of a "racetrack" covering approximately 12 turns of one side of two azimuthally adjacent coils. Thus the parallel or series connection of two "opposite heaters" (H1&H3 or H2 & H4) in a given layer provides protection to all four magnet quadrants.

During the course of the model program there were four heater parameters that were studied: 1) heater location, either between the inner and outer layer or between the outer layer and the collar, as shown in figure 1 and 2, 2) the amount of heater insulation between the coil and the heater, 3) heater width, i.e. how many coil turns are covered by heater and 4) longitudinal distribution of the stainless steel heater centers by masking the stainless steel with a thin layer of copper. The optimization is further discussed in chapter 3.

A summary of the heaters parameters for all the magnets are shown in table 1. As can be inferred from the chronology of the magnets, the first heaters were bare stainless steel strips located between the inner and outer coil (as shown in figure 2). At the end of the project, the heaters were moved to the outer layer and contained distributed resistance centers. The insulation between and coil and the heater was reduced. The heater width remained about the same.

Of particular interest are the heaters used in HGQ08-9. These heaters were provided by CERN and have widths and insulation thickness that are consistent with the heaters for the CERN dipole. The primary difference between the two designs is the longitudinal

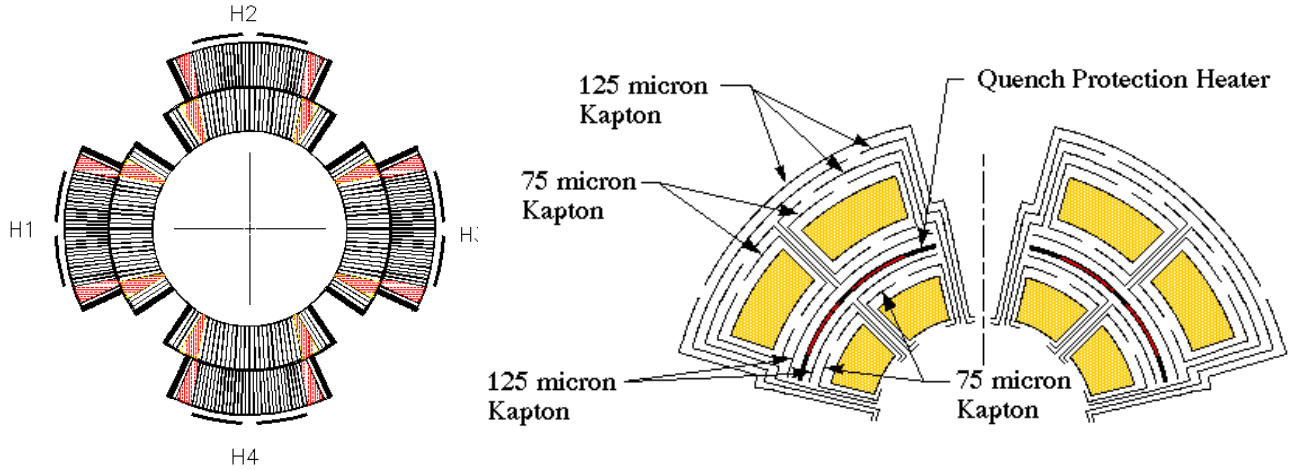


Figure 1 a) Coil geometry showing azimuth location of quench heater (H1-H4) for the outer layer heaters. b) Insulation scheme showing location of "inner layer" heaters

resistance distribution. In HGQ08 there is 1 Stainless steel segment followed by 2 copper segments, while HGQ09 there is 1 Stainless steel segment followed by 1 copper segment. The segment length is ~110 mm or 1 cable transposition pitch. The heater in HGQ09 covers more coil area, while HGQ08 heater has a substantially higher peak power density (for the same power supply voltage and capacitance). Our plan is to use one of the two heater geometries for the prototype and production magnets.

TABLE I.
STRIP HEATERS IN HIGH GRADIENT QUADUPOLE MODELS

Magnet	Position	Element (all 25 μ m thick)	Insulation
HGQ01	Inter	Stainless steel 15.9mm wide	325uM
	Outer	None	N/A
HGQ02	Inter	Stainless steel 15.9mm wide	325uM
	Outer	Stainless steel 15.9mm wide	350uM
	Inter	Stainless steel 15.9mm wide	325uM
HGQ03 & HGQ05	Outer	15.9 mm wide with copper plating 38 mm etched areas at 114 mm intervals.	350uM
	Inter	None	N/A
HGQ06	Outer	12.7 mm wide with copper plating 610 mm etched areas at 1930 mm intervals.	250uM
	Inter	None	N/A
HGQ07	Outer	22.2 mm wide with copper plating 610 mm etched areas at 1930 mm intervals.	250uM
	Inter	None	N/A
HGQ08	Outer	15 mm wide with copper plating 120 mm etched areas at 360 mm intervals.	250uM
	Inter	None	N/A
HGQ09	Outer	15 mm wide with copper plating 102 mm etched areas at 204 mm intervals.	225uM
	Inter	None	N/A

Test Program

The tests were performed at the Fermilab Technical Division Vertical Magnet Test Facility [ref]. VMTF utilizes a vertical Dewar designed to operate with superfluid and normal helium at 1.1 atmosphere. Magnet current is supplied by a 16 kA DC power system with an energy extraction circuit (dump resistor). The strip heater and the spot heater voltage are supplied by a 0-450 V Heater Firing Unit (HFU). The capacitance of the system can be set in 4.8 mF increments up to 19.2 mF. The cold resistance of a stainless steel heater of width 15.9 mm is about 5.5 ohms. The stainless steel heaters were typically operated in parallel, while the distributed resistance heaters were operated in series. The RC time constant for the former tests was 40 ms while for the latter tests the time constant was set to approximately 80 ms. The 80 ms time constant was chosen because this is the value in LHC operation, using a 7 mF capacitor bank and two full length heaters connected in series with a 33 percent stain less steel/copper distribution.

Heater Performance

Heater performance is characterized by V_{min} , the minimum voltage (or energy) required to initiate quench, t_{fn} , the time between quench heater firing and resistive voltage initiation, and the quench integral, the time integral of the square of the quench integral normalized to 10^6 , measured in MIIT's.

V_{min} level determines the voltage requirements for the heater power supplies. Figure 2 shows the measured V_{min} for stainless steel heaters in parallel and the series circuit of the distributed resistance heaters in HGQ06-HGQ09. HGQ06, HGQ07 and HGQ08 heaters have a similar ratio of stainless steel to total area (approximately 33 percent) but different widths. HGQ09 has a stainless steel percentage of 50 percent) As shown, the voltage for the distributed heaters is slightly reduced relative to that for the stainless steel heaters. The HGQ07 voltage reduction is as expected when one folds in the width of the heater. (22 mm vs. 15.9 mm) In fact the peak power surface densities at these V_{min} voltages are comparable. The voltage savings are not as significant as one would expect for the narrower HGQ06,8 and 9 heater. A possible explanation for this is that the narrower heater primarily covers turns near the low field midplane and thus requires a larger power density to be effective.

Finally, for HGQ08 and HGQ09 the minimum voltage was determined at 800 amps, which corresponds approximately to the current at the LHC injection. The required voltage for quench initiation is less than 200 and 270 volts, scaling to full scale magnet this would corresponds to approximately 600/800 volts for the LHC tunnel. This is well below the 900 V power supply setting.

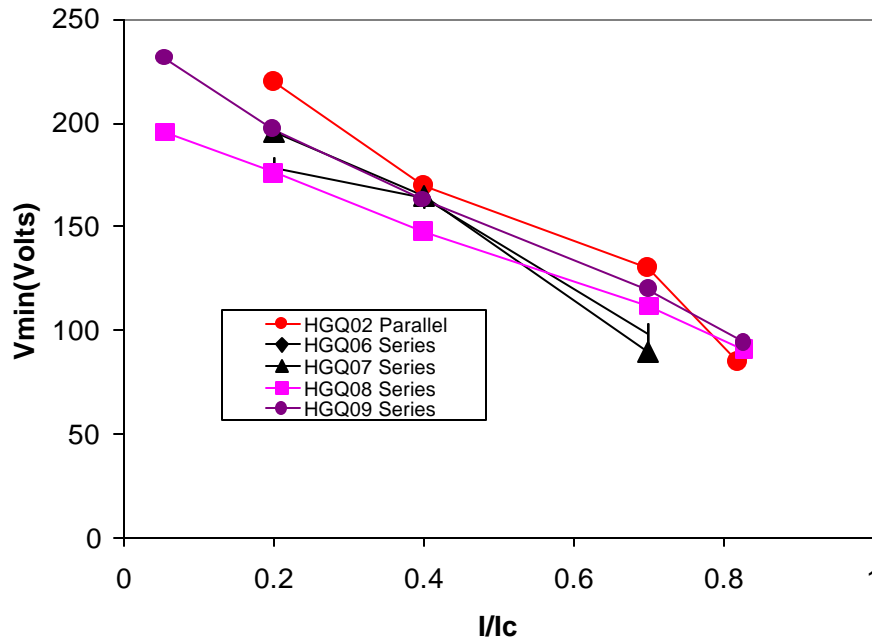


Figure. 2. Minimum voltage per heater circuit to initiate a quench vs. normalized excitation current.

The t_{fn} is a good measure of the heater efficacy. Low values of t_{fn} result in lower quench integral, which in turn translates into lower coil peak temperatures.

In HGQ01 and HGQ02 we were primarily concerned with the location of the heaters. Figure 3 is a comparison of t_{fn} for stainless steel strips heaters in the outer and inner layers, as a function of heater power supply voltage. As can be seen there is essentially no difference in the initiation of resistive voltage between the two heater locations. Note that the t_{fn} for both inner and outer heaters is set by the resistive growth in the outer coil. We observed that for the inner strip heater, the t_{fn} contribution from the inner coil is retarded relative to the outer coil, despite the fact that the inner coil is in a higher magnetic field. This delay is likely due to the inner coil cooling channels which increase the liquid helium wetted surface between the inner strip heater and the inner coil. The inner and outer heaters have comparable t_{fn} for the outer coil because the heater insulation is nearly identical and the magnetic field across the outer coil conductor is fairly uniform in the vicinity of the heaters.

Figure 4 is a comparison of outer heaters with different heater widths and copper plating. While there is quite a bit of data in these plots several patterns emerge. First, as expected, for a given heater and power density, the t_{fn} decreases with excitation current. Second, while there is a considerable spread of values at $I/I_c = 0.2$, they all converge at high current to a t_{fn} of 20-30 ms. In general, and independent of the resistance distribution, the larger the power density, the smaller the t_{fn} for a given current. Finally, the wider the strip, the smaller the t_{fn} . A plausible explanation for this is the following: for all heaters, one edge is placed azimuthally within the first two midplane turns. Wider heaters not only cover more turns but covers turns in the higher field region. These turns have a lower temperature margin and should respond more quickly to the heater energy pulse.

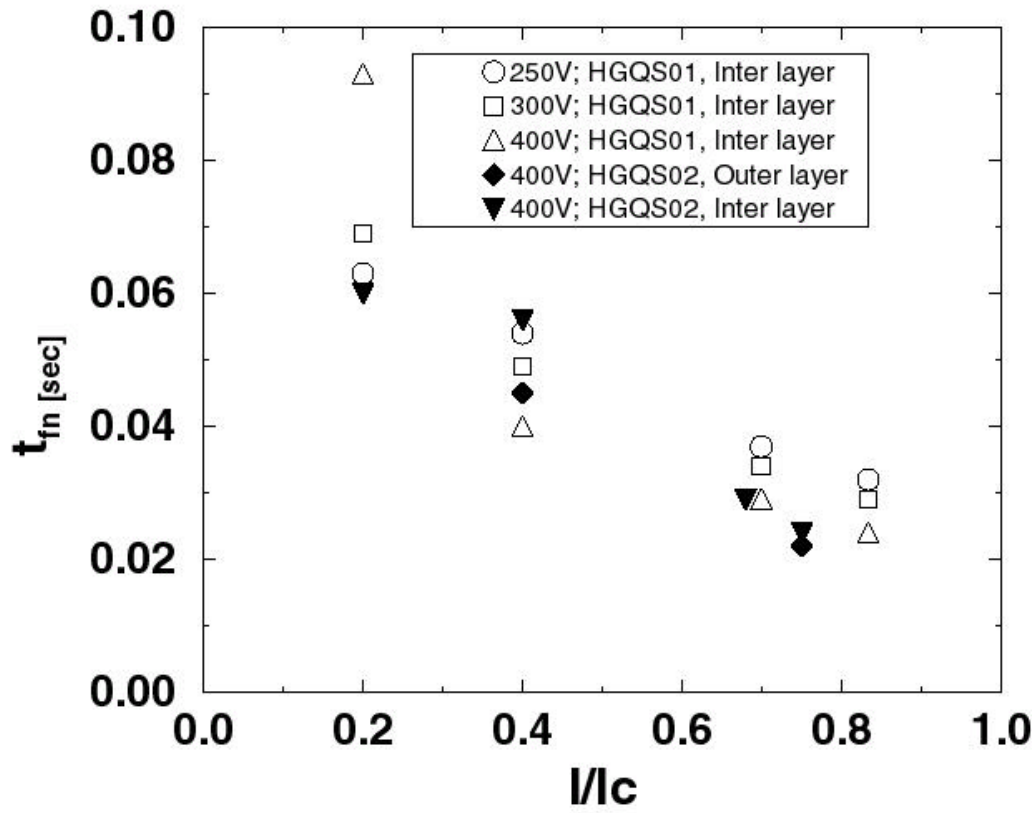


Figure 3 Inner vs. outer layer stainless steel heaters, for fixed heater power supply voltages.

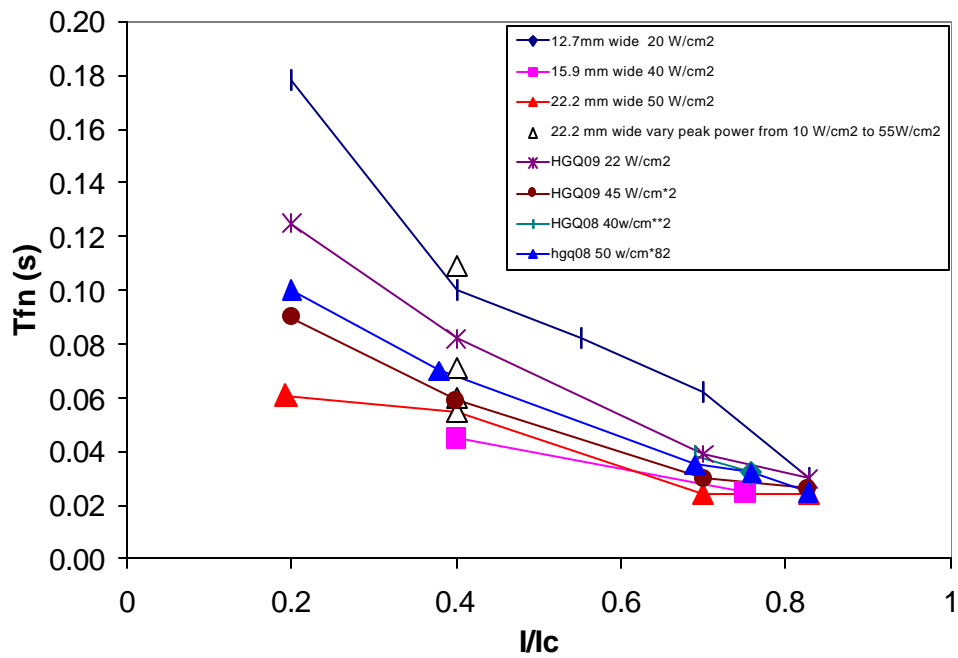


Figure 4 t_{fn} for outer layer heaters as a function of normalized current and power densities.

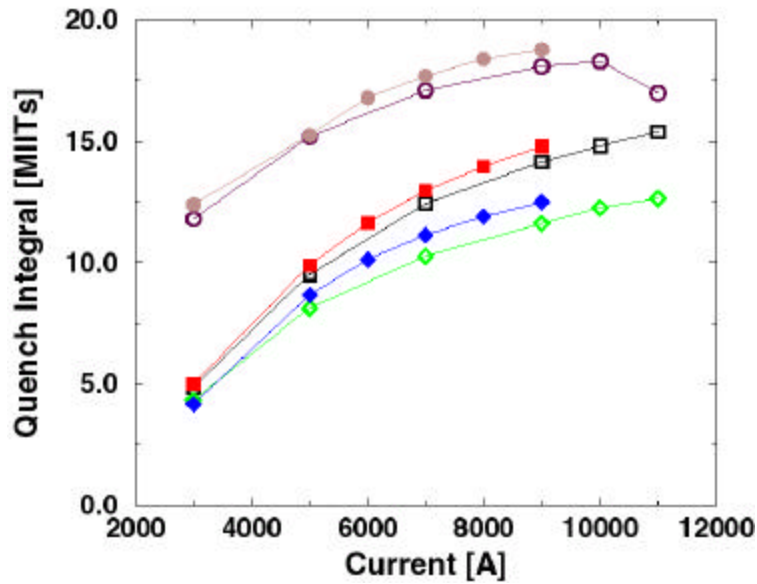


Figure 5. Quench integral (QI) for outer layer (solid) vs. inner layer (open) strip heaters Circles: QI from spot heater quench initiation, Squares: QI from quench detection, Diamonds: quench integral from strip heater resistive voltage onset.

The quench integral can be directly related to the peak temperature in the coil. Contribution to the quench integrals come from the time to detect the quench, the time from the heaters become effect (related to t_{fn}) and the time for the energy in the coil to be dissipated. Figure 5 shows the quench integral expressed in MIIT's as a function of applied current for quenches induced with a inner layer pole turn spot heaters and protected either with outer (solid symbols) or inner (open symbol) strip heaters. There are three families of curves; the upper set represent the quench integral starting time at the onset of the spot heater induced resistive voltage, the middle set are the quench integral with a starting time corresponding to the 300 mV quench detection and strip heater firing, and the lower set represents the quench integral from the onset of voltage growth in the outer coil due to the strip heaters. The full quench integral has a peak value of 19 MIIT's using either protection heater. This corresponds to a peak temperature of about <200 K in the inner coil. Note that inner layer heater is only slightly more effective than the outer layer heater. These data indicate that the quench detection time of 300 mV is a major contributor to the quench integral.

Next we compare in figure 6 the relative effectiveness of the distributed resistance heaters for HGQ08 and HGQ09, as a function of peak power density using manually induced system trips. These trips shut off the power supply and fire the strip heaters and start the MIIT's clock. This corresponds roughly to the second family of curves shown in figure 5. The values of 55 W/cm^2 and 22 W/cm^2 were chosen to correspond to the power density for HGQ08 and HGQ09 style heaters, when extrapolated to a full scale 5.5m long magnet using the CERN 900 V, 7 mF heater power supply. For a given heater supply the quench integral decreases with increasing power, as expected. The HGQ08 heaters perform better than the HGQ09 heaters, especially at their nominal LHC power densities.

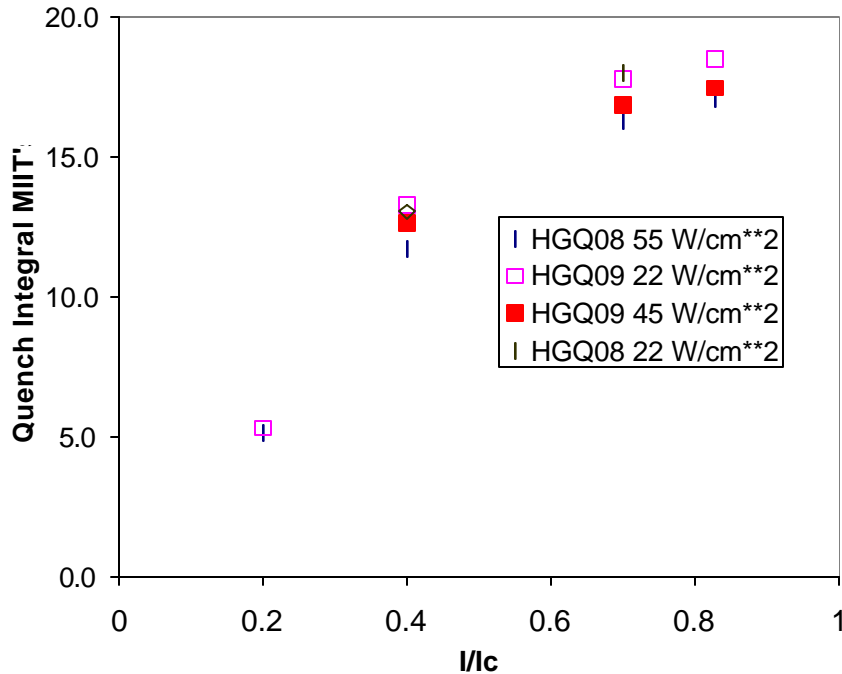


Figure. 6. QI vs. normalized excitation current for "manual trip" quenches.

Peak Voltage

The peak voltage is defined as the highest voltage measured from any of the eight coil leads relative to the magnet leads. This voltage develops because of coil to coil variation in t_n and coil to coil differences in RRR. The design goal for these magnets was to limit this voltage to 1000 V for a full-scale magnet [ref]. Heater peak voltage is shown in figure 7, for a distributed heater and a stainless steel heater. The results for the other distributed heaters show very similar results. The measured voltages to ground are low: less than 30 V for 1.9 m long magnets. Extrapolating to a full-scale magnet with two redundant heater circuits, the voltage is will not exceed 200 V. The results for the "adjacent" heater configuration is also included in Figure 7. Referring to figure 1, this would be the case where H1 & H2 were connected in series (note: this configuration would not even be considered unless there were problems with 1 or more of the strip heaters). Even under this case, with no heater protection in one quadrant, the peak voltage is less than 120 V, which would translate to less than 400 V for a full-scale magnet.

Using these data, one can attempt to model the effects of having two 5.5 m long magnets connected in series, using as input the measured resistance and inductive voltage growth from the heater induced quenches. We varied the starting time of the resistance growth within the measured t_n . We also studied the possibility of a resistive voltage imbalance between the two magnets due to a 100% difference in the conductor RRR. We estimate that the peak voltage growth would not increase by more than a factor of two under these conditions thus still producing an acceptably low voltage.

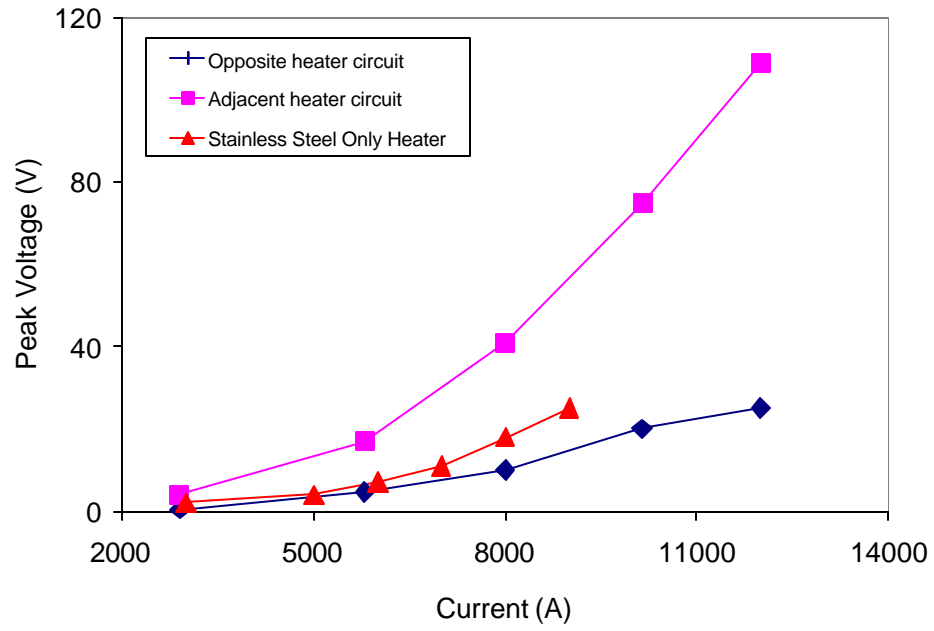


Figure. 7. Peak voltage as a function of excitation current. For stainless vs. distributed heaters.

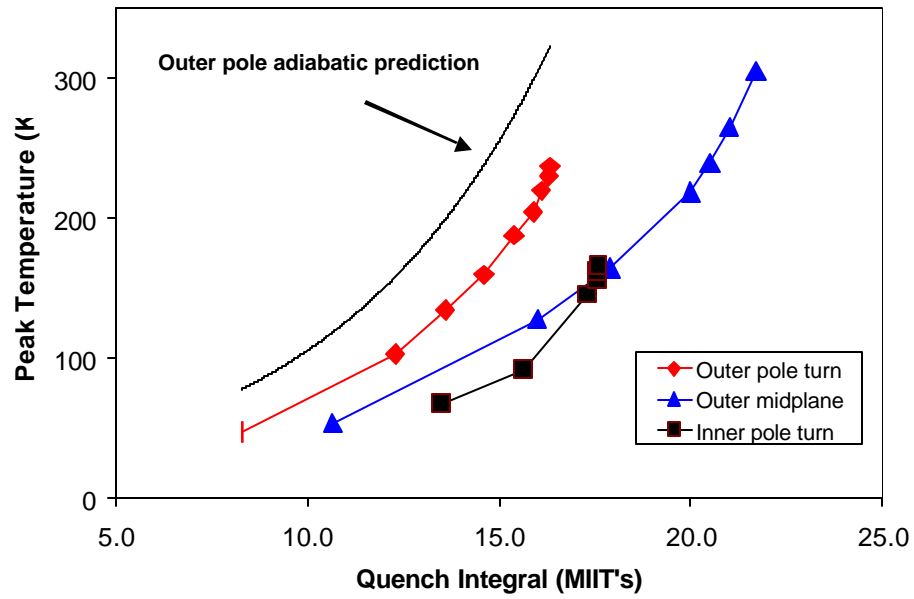


Figure. 8. Measured peak temperature vs. the quench integral

Peak Coil Temperature

The peak coil temperature, assumed to be in the origin of the spontaneous quench is estimated in two ways. First, the temperature can be simply related to the time integral of the square of the excitation current (quench integral), using an adiabatic temperature model. The other method is to measure directly the cable resistance adjacent to a spot heater. The measured resistivity, dominated by the resistance of the copper is then directly related to the cable's local temperature. The design for the magnet was to limit this peak temperature to less than 400K [8].

Figure 8 shows the measured peak temperature as a function quench integral for representative magnets. The spot heaters for these tests are located in three locations, 1) the pole turn of the inner coil, 2) the pole turn of the outer coil, and 3) the outer coil midplane turn in the end of the magnet. In all cases, increasing quench integral represent higher excitation currents and therefore high magneto-resistance at the onset of the quench. In general the inner cable has a lower peak temperature vs. quench integral curve since the inner cable has more copper and superconductor. For the outer cable, the pole turn temperature is higher than the midplane temperature for a given quench integral due to the pole turn being in a higher field region. This explains the greater sensitivity of the pole turns to heat generation. In all cases the shape of these curves is well predicted by the adiabatic calculation. As expected, the scale of the adiabatic prediction is more pessimistic.

Finally, the peak temperature is plotted directly against the peak excitation current. Figure 9 shows this relationship for spot heater quenches originating in the high field region (pole turns) of the inner and outer coils. For quenches originating in the inner coil, the peak temperature is approximately 150 K. For the outer pole turn (measured in HGQ06), the peak temperature for quenches in the 12 kA operating range is less than 250K.

Quenches in the outer coil midplane will have the highest peak temperature, thus the studies on the last 3 magnets were centered on this extreme case. The results of the study are shown in figure 10. The power density for HGQ07 and HGQ08 were again chosen to represent those in the LHC operation. The peak temperature for HGQ08 was lower than that of HGQ07, even though the HGQ07 covered more surface area with the same RC time constant and power density. This improved performance is consistent with the quench integral results in figure 8. Note that for HGQ08 the cable has a very low interstrand resistance, which could accelerator the quench process through the so called "quench back" mechanism. In both cases the peak temperature was approximately 300K.

The results in HGQ09 where more interesting. There were two heaters located in the midplane pole turn on two different coils, each yielded different results. One heater produced peak temperatures comparable to the HGQ07 and HGQ08. For the peak power density of 45 W/cm², the peak temperature was less than 300K. The other heater produced considerably heater peak temperature, of approximately 360 K. The difference in the temperatures can be attributed to the time required to detect the quench, there is a 20 mS difference in the quench detection time. This difference cannot be explained by coil to coil differences in RRR.

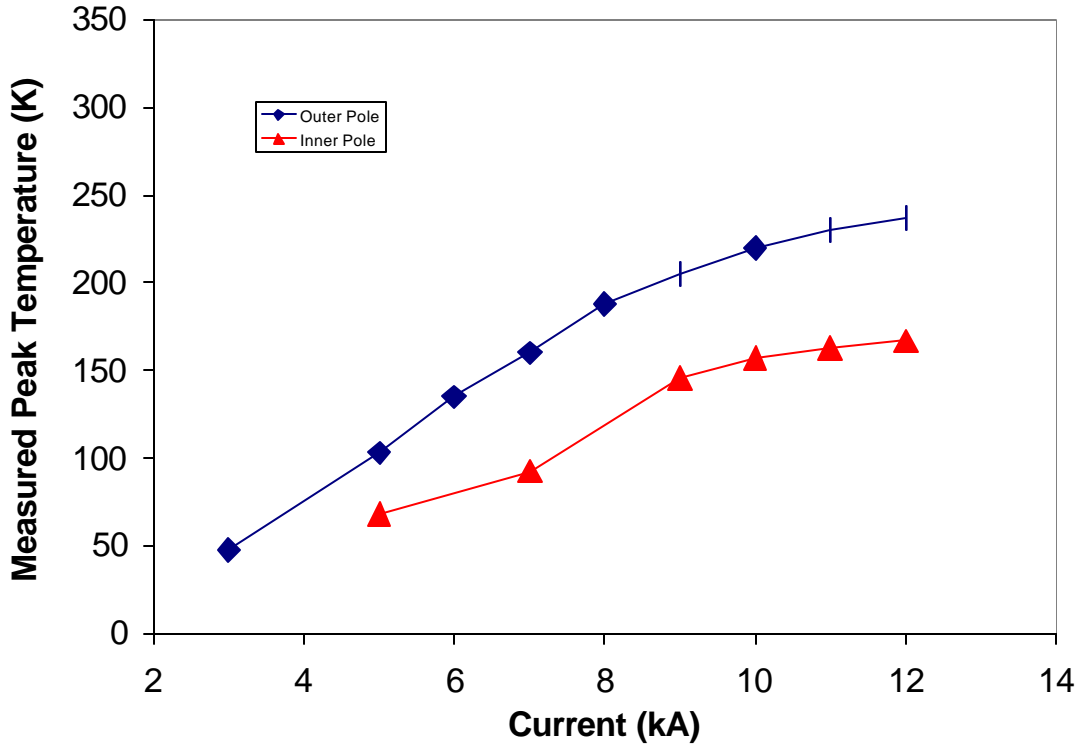


Figure. 9. Comparison of measured peak temperature vs. excitation current. For spot heater induced quenches in the inner and outer coil pole turn.

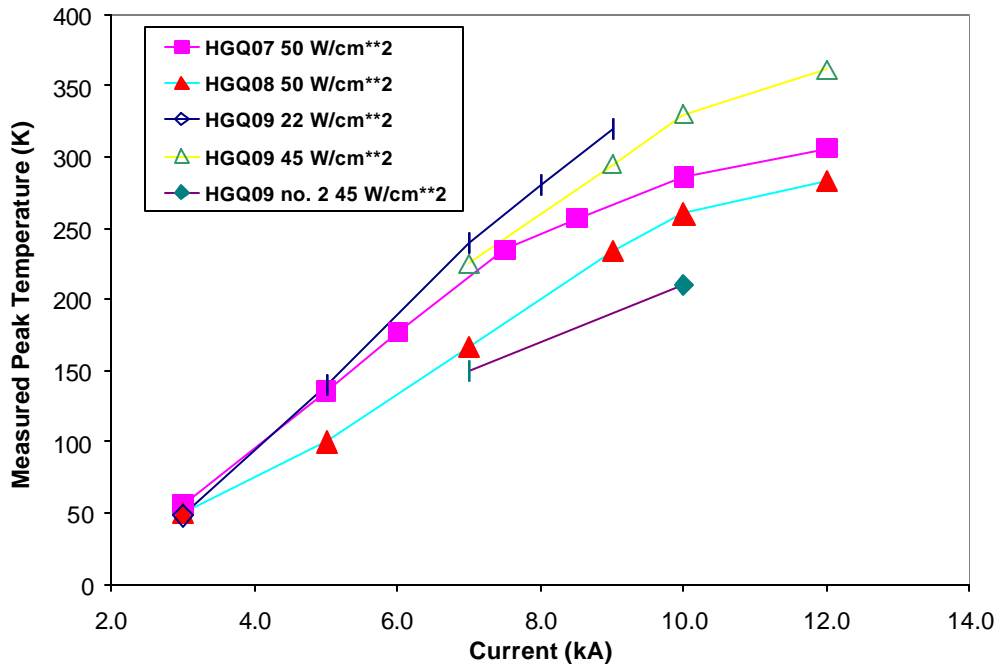


Figure10. Peak temperatures for outer coil midplane quenches.

Finally, we note that the inner coil direct measurements were made with the 38-strand conductor. One would expect a slightly higher peak temperature with the 37-strand conductor due to the decrease in the copper and superconductor. Using the adiabatic calculations to scale, the peak temperature is predicted to increase by approximately 10% to 165 K.

4. Conclusion: Magnet Protection/Heater Studies

Strip heaters of various geometries, insulations and locations were tested over the full range of excitation energies and currents. Worst case peak temperature and peak voltages to ground are within design limits.

The outer layer heater was chosen over the inter layer heaters, as they both work well but the outer layer heaters are much easier to install. Wider heaters work slightly better than narrow ones, with noticeable degradation from the 12.2 mm heater vs. the wider heaters. We strongly suspect that these narrower heater would be more effective if they were placed azimuthally closer to the pole region.

The insulation between the coil and heater was systematically reduced over the course of the program. It is difficult to quantify the effect of this as these reduction were always done while changing other heater parameters. The effect reducing 25-100 microns of insulation seem to be small compared other parameters since all heaters seem to have similar t_{fns} at the highest currents.

Concerning distributed resistance: The 33 percent stainless appear to work just as well as the 50 percent heaters at the same power density. Thus quench velocity, required to 'fill in' the longitudinal portions not covered by the heaters, appears to be sufficient. Peak power appears to be more important to heater performance than longitudinal heater coverage. Given the power limitations imposed in the tunnel, the lower percentage of stainless steel in the HGQ08 heater allow for higher peak power which has been shown to reduce the MIIT's and corresponding peak temperatures.

5. Bus bar studies

- 1) Scope of IR Quadrupole Bus bar Test Series

As stated above, it is envisioned that the bus-bar will be protected with the same quench protection system at the magnets. When the resistive voltage exceeds the quench detection threshold of 300-500 mV, the power supplies will be turned off and the magnet heaters will be fired. Based on the magnet protection studies presented in this chapter, the bus-bar will then experience an additional quench integral of 15-20 MIIT's after the quench is detected. The bus-bar design consists of a superconducting cable used as well for the inner layer of the Fermilab IR quadrupoles, soldered to similar Rutherford-type cables as stabilizers. The bus-bar has to satisfy the following (antagonistic) requirements:

- Maximum stability against quenching during normal operation;
- minimum temperature rise in the bus-bar after a quench ($T_{\text{peak}} < 300 \text{ K}$);
- maximum quench propagation velocity to accelerate detection of quench;

A program to test several bus-bar prototypes in operating conditions was proposed and presented. Table 2 resumes the lay-out of the bus-bar tests conducted within the framework of the IR quadrupole short model program.

Test	- Samples	- Objective of test
1	A: 2 supercond. stabilizer, soldered B: 2 supercond. stabilizer, insulated	Difference in v_q between A and B, general performance (quench stability, temperature rise during quench)
2	C: 2 supercond. stabilizer, soldered D: 1 supercond. stabilizer, soldered	v_q , R(MIIIs), performance in magnet environment, quench-stability
3	E: 2 copper stabilizer, soldered F: 1 copper stabilizer, soldered	v_q , R(MIIIs), performance in magnet environment, quench stability

Table 2: Bus-bar test series. The design of the samples refers to one superconducting inner layer LHC IR quadrupole cable with additional stabilizer.

Test 1 [ref TD-99-059] was designed to test two design variations: in case A all three identical cables were soldered together, whereas in case B the pack was divided into a soldered 2-conductor pack and the main conductor with an insulating polyimide foil in between. The difference in quench propagation between the two alternative arrangements was investigated. The measurements revealed that the quench propagation velocity is equal in both configurations. For future tests the soldered version was retained.

Test 2 [ref TD-00-006] was designed to measure the effect of MIIIs accumulation and to test the bus-bar together with a model magnet. The test station's quench detection circuits were modified to allow the bus-bar to develop higher temperature and resistance after a quench. A bus prototype with only one stabilizer (case D) was tested as well. Both samples performed well within the stipulated limits.

In test 3 [ref TD-00-???) the stabilizers were made from pure copper strand cable, repeating the sequence of test 2. The samples again performed well and a proposal for a final bus-bar design was issued.

The performance of the bus samples was tested by submitting samples of the bus to operational conditions and characterizing them with respect to quench propagation velocity and voltage profile during normal zone growth.

The following resumes the results of the bus-bar experiments and leads to the final specification of the bus-bar design.

- 2) *Experimental Setup*

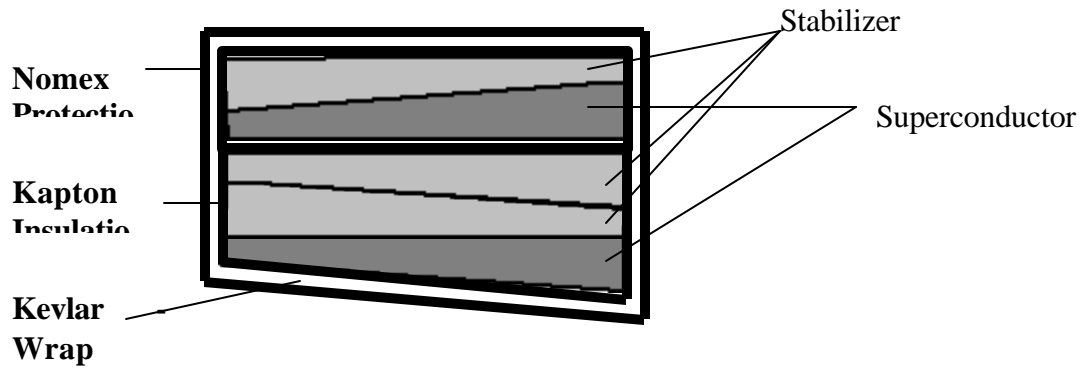


Figure 11: Test series 2 LHC IR bus-bar assembly: The so called 2-bus and 3-bus form the positive and negative branch of the magnet power leads.

Figure 11 shows the cross-section of the bus-bar assembly used in test 2 & 3. The 2-bus (go-) and 3-bus (return-) were separately insulated with a single 50% overlap wrap of 75 μm adhesive Kapton[®], followed by a shrink-sleeve wrap and firmly attached together with a tight wrap of Kevlar[®] string to prevent motion due to repulsive force between the bus-bars. Both bus-bars were equipped with spot-heaters to trigger quenches, and voltage taps along four 4-inch long segments to monitor quench propagation.

- 3) *Results of the Bus-bar Test-Series*

- 3.1) *Quench Propagation Velocity Measurements*

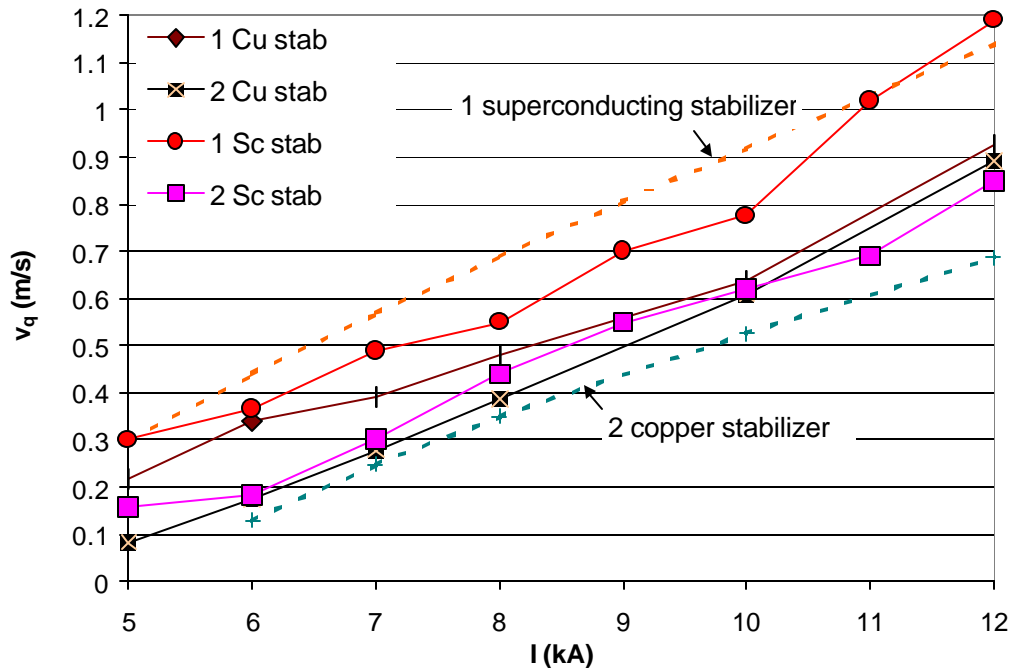


Figure 11: Results of bus-bar quench propagation velocity measurements in test-series 2 & 3.

The quench propagation velocity is measured using the time of flight method. The magnet is ramped to the chosen current and a quench is initiated in a voltage segment (segment 0) with the spot heater. The quench propagates to neighboring segments. The quench propagation velocity is calculated from the known length of the voltage segment and the time it takes the voltage onset in the conductor to travel through the voltage taps delimiting this particular segment. The measured quench propagation velocity data for the bus prototypes at different currents are shown in Figure 2. The fits of the experimental curves in Figure 11 (dashed) were obtained with Dresner's quench propagation velocity formula [ref Dresner].

3.2) Quench Integral vs. Temperature Measurements

The calculated peak temperatures as a function of quench integral (QI) were compared to experimental data obtained during a series of tests in which the quench detection threshold was increased such, that the bus-bar could operate at higher quench integrals and rise to higher peak temperature. The (adiabatic) quench integral is defined in equation 1.

$$QI(T_{peak}) = 10^{-6} \int_0^{\infty} I_t^2(t) dt = 10^{-6} \frac{I}{I+1} A^2 \int_{T_0}^{T_{peak}} \frac{c_{pcomp}(T')}{r_{Cu}(T')} dT' \quad \text{MII}ts \quad (1)$$

The quench integral can be calculated either from the temporal current profile (middle term in equation 1) or from basic material parameters (right term in equation 1).

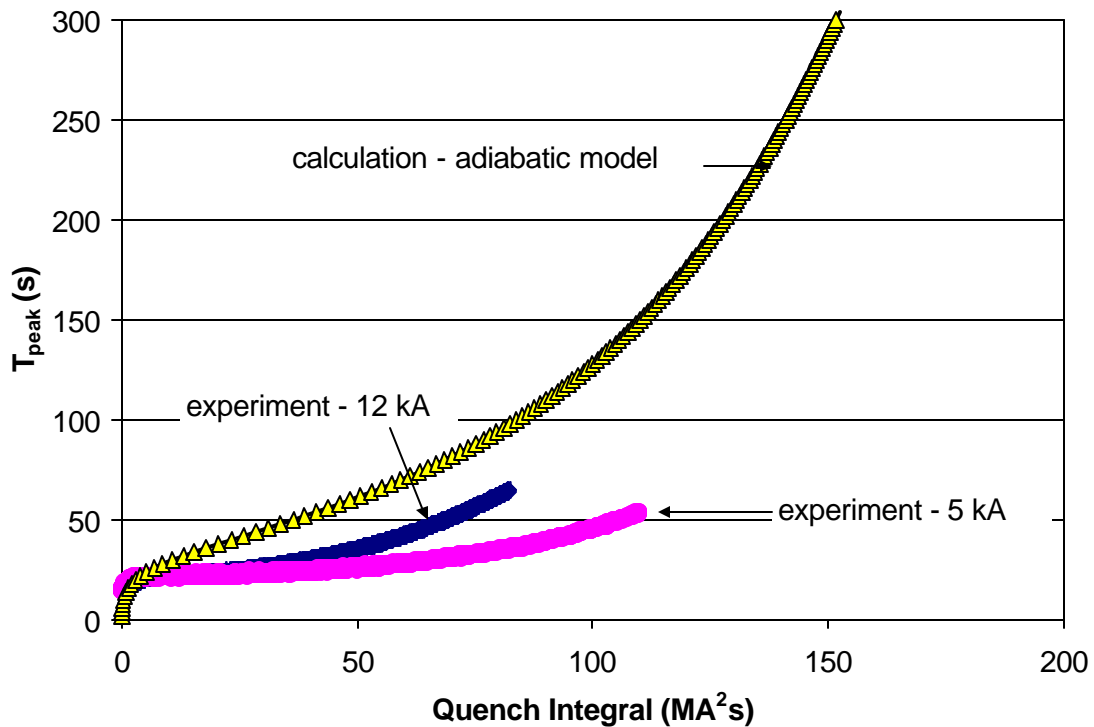


Figure 13: Experimental and calculated T_{peak} (QI) for bus with 1 Cu stabilizer at 5 & 12 kA.

To convert the experimental voltage vs. time data to temperature vs. quench integral data the following procedure was followed: The voltage data of the segment quenched originally by the spot heater were converted into a resistivity (knowing current, Cu cross-sectional area and the length of the segment), assuming that the segment was isothermal over its full length. Figure 13 shows a comparisons for a bus sample with 1 copper stabilizer at low and high current. In general it was found, that the higher the current the better the agreement between the adiabatic model and the experimental data. It seems that with decreasing currents the peak temperatures for a given number of MIIts decrease (and thus the T_{\max} vs. QI curve diverges from the adiabatic limit the lower the current). The current dependence of the above mentioned effect hints toward a cooling effect.

- 3.3) *Quench Detection Voltage vs. Quench Integral*

It can be shown that the voltage generated along the bus as a function of quench integral is given by:

$$V_q = I_t r_{Cu} (MIIts_{\max}) * L_{MPZ} (I_t) \frac{1}{A_{Cu}} + 2 \cdot 10^6 \frac{v_q}{I_t A_{Cu}} \int_0^{MIIts_{\max}} r_{Cu} (MIIts) d(MIIts) \quad (2)$$

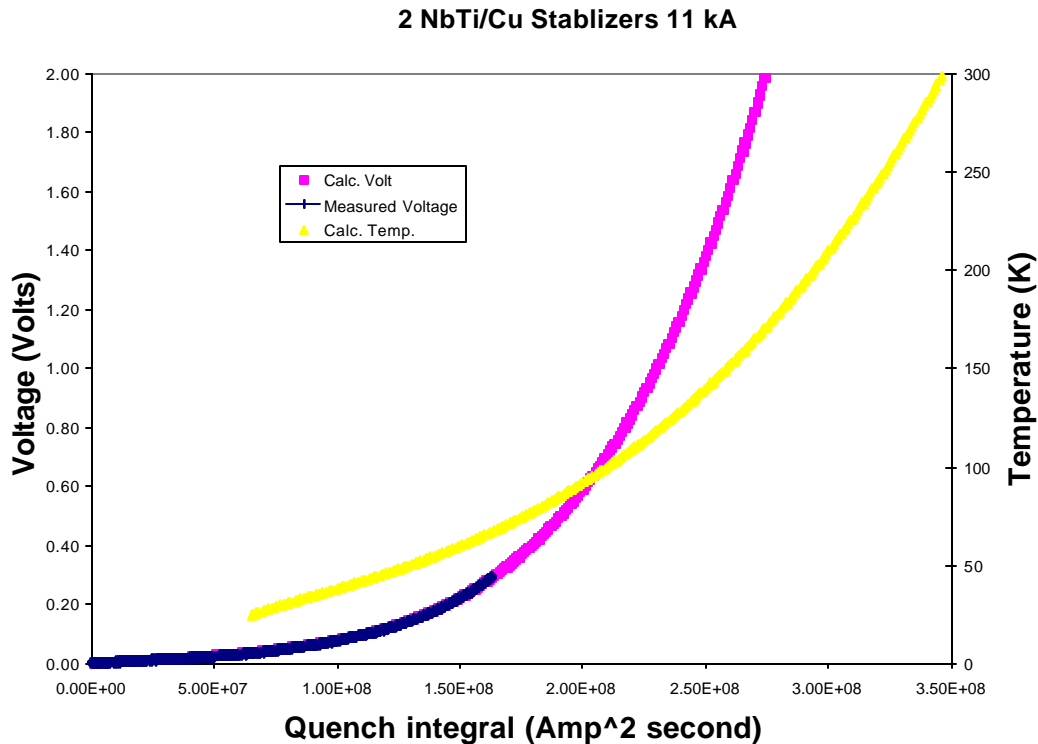


Figure 12: Comparison of calculated and measured voltage development during a quench. 3-bus, (2 superconducting stabilizer), 11 kA, 1.9 K.

The voltage in equation 2 is a superposition of:

- the voltage generated in the initially quenched zone of length L_{MPZ} (Minimum Propagating Zone) and
- the voltage rise generated in the rest of the bus through quench propagation.

The dependence of resistivity on quench integral, used in both terms of this equation is determined directly from the measured resistance growth of a short segment of the cable near the quench location. The polynomial $\rho_{Cu}(MIIts)$ fit is inserted together with the experimental quench propagation velocities into equation 2 to calculate the voltage. This procedure allows to extrapolate the voltage-temperature relation beyond the experimental range. As an example the voltage vs. peak temperature characteristic of the bus-sample with 2 Sc stabilizer is shown in Figure 14.

- 3.4) Peak Temperature vs Magnet Current

The peak temperature vs. quench integral and the quench voltage vs. quench integral relations can be combined to yield answers to the crucial questions of bus-bar design. The most important among them is the peak temperature in the bus after a quench for a given quench detection threshold voltage. Figure 15 shows such plot for a quench detection threshold voltage of 300 mV, indicating that all bus-bar prototypes remain well within the stipulated temperature limits.

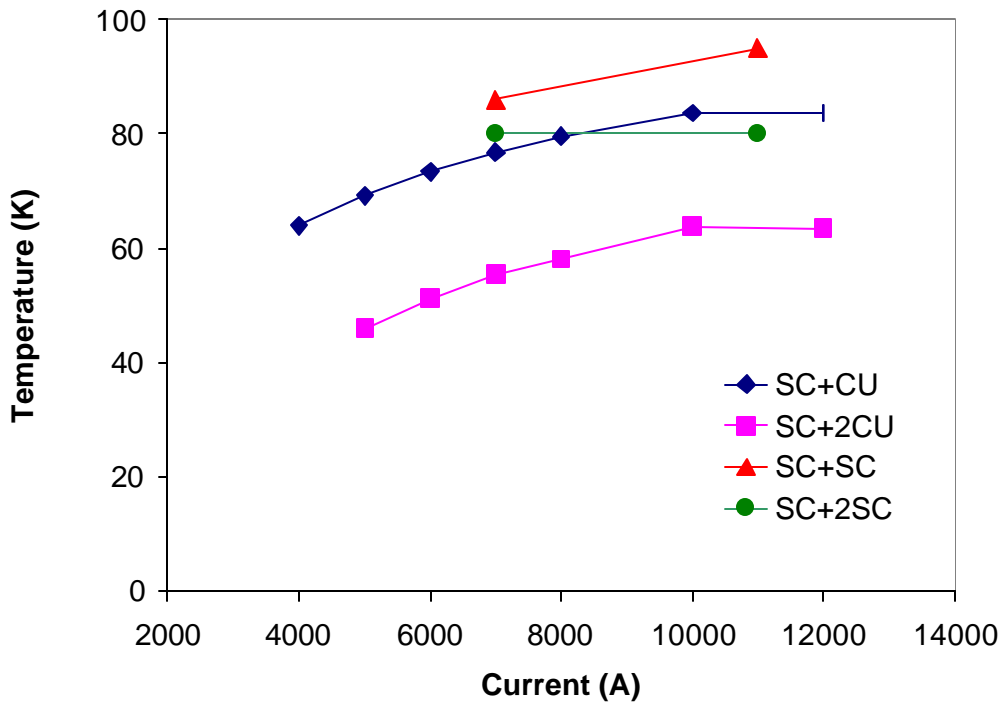


Figure 15: Peak temperature in bus as a function of magnet current after a quench in different bus samples at a quench detection threshold voltage of 300 mV (including 20 MIIts for magnet ramp down).

- **4) Conclusions**

The bus-bar samples tested in this test-series are suited for operation in the LHC interaction region environment. The assembly of the bus-bar into the magnet was practiced. The bus-bars did not quench spontaneously during the entire test of the magnet, which involved accelerator type current cycles as well as long dwell times at operation current. This shows that the mechanical support is sufficient to suppress mechanical disturbances exceeding the stability limit of the bus. It also shows that there is no major magnetic coupling between the bus-bar and the magnet. The amount of copper-stabilizer in the bus cross-section is adequate for the quench detection threshold voltages foreseen for the LHC IR quadrupole quench protection system. All bus-bar samples would stay within less than 100 K after a quench. Tight space requirements in the KEK quadrupoles and demands on bus-bar flexibility suggest the sample with one copper stabilizer to be the candidate for the final interaction region bus-bar design. Table 3 lists the characteristics of this bus-bar design.

Main bus	HGQ inner type cable: Cu/Sc=1.3, 38 strands, 0.808 mm diam.
# of stabilizers	1
Stabilizer type	HGQ inner type cable made from Cu strands
Cross-sectional surface	38.97 mm ²
Copper cross-section	27.96 mm ²
Width and thickness	15.4 mm wide, 2.91 mm mid-thickness
Insulation	250 μm Kapton®
Cu/Sc ratio	2.538
RRR	100
Quench propagation velocity at 12 kA	0.9 m/s
Quench propagation velocity at 8 kA	0.5 m/s
Quench propagation velocity at 5 kA	0.2 m/s
Peak temperature after a quench at 12 kA ($V_{qdet}=250$ mV)	60 K
Peak temperature after a quench at 8 kA ($V_{qdet}=250$ mV)	54 K
Peak temperature after a quench at 5 kA ($V_{qdet}=250$ mV)	45 K
Cryo-stability current threshold	4 kA

Table 3: Geometrical and operational characteristics of the LHC IR bus-bar prototype.

